K_d determinations

We made K_d measurements by equilibrium dialysis or spin-filtration[14], with equivalent results, using purified MBP fusion proteins exchanged into selection binding buffer by gel filtration. We determined the K_d for ATP and ATP analogues by displacing bound ^{32}P-ATP from the protein by increasing concentrations of competitor. The stoichiometry of the protein–ATP interaction was determined by a procedure adapted from ref. 15.

Deletion analysis

Deletion analyses were done with both DNA-tagged proteins[5] and MBP fusion proteins. Primers designed to anneal to specific internal parts of clone 18-19 were synthesized. For the DNA-tagged proteins, 5′ primers encoded the TMV enhancer and T7 promoter sequences, with MD as the common N terminus, and 3′ primers encoded the peptide MGMSGS as the common C terminus. These primers were used to generate truncated mRNA-displayed proteins from clone 18-19 as described above. Subsequent purification on oligo(dT)cellulose, incubation with RNase A, and a second purification on oligo(dT)cellulose yielded purified DNA-tagged proteins[5]. The fraction of each DNA-tagged protein that was competent to bind ATP-agarose was determined under selection conditions as described above. MBP fusion proteins were generated in a similar manner by PCR of internal fragments of the protein 18-19 coding sequence, followed by cloning into the MBP fusion expression plasmid, expressing and purifying the MBP fusion deletion constructs, thrombin cleavage to release the deletion fragment from the MBP, and measuring solution K_d by equilibrium dialysis or spin-filtration.

Gel-filtration chromatography

Protein 18-19 was expressed as an MBP fusion as described above. The time taken for the protein to traverse a Sepharose 200 FPLC column in selection binding buffer was measured on an AKTA FPLC by analysis of column fractions on silver-stained SDS–PAGE gels. The molecular weight of the protein was calculated by comparison with known protein standards.

Received 21 September 2000; accepted 16 January 2001.

1. Roberts, R. W. & Szostak, J. W. RNA-peptide fusions for the *in vitro* selection of peptides and proteins. *Proc. Natl Acad. Sci. USA* **94,** 12297–12302 (1997).
2. Sassanfar, M. & Szostak, J. W. An RNA motif that binds ATP. *Nature* **364,** 550–553 (1993).
3. Wilson, D. S. & Szostak, J. W. *In vitro* selection of functional nucleic acids. *Annu. Rev. Biochem.* **68,** 611–647 (1999).
4. Cho, G., Keefe, A. D., Liu, R. L., Wilson, D. S. & Szostak, J. W. Constructing high complexity synthetic libraries of long ORFs using *in vitro* selection. *J. Mol. Biol.* **297,** 309–319 (2000).
5. Wilson, D. S., Keefe, A. D. & Szostak, J. W. *In vitro* selection of high affinity protein-binding peptides using mRNA display. *Proc. Natl Acad. Sci. USA* (in the press).
6. Freedman, L. P. *et al.* The function and structure of the metal coordination sites within the glucocorticoid receptor DNA binding domain. *Nature* **334,** 543–546 (1988).
7. Altschul, S. F. *et al.* Gapped BLAST and PSI-BLAST: a new generation of protein database search programs. *Nucleic Acids Res.* **25,** 3389–3402 (1997).
8. Considine, D. M. (ed.) in *Van Nostrand's Scientific Encyclopedia* 7th edn, 3067 (Van Nostrand Reinhold, New York, 1989).
9. Liu, R., Barrick, J., Szostak, J. W. & Roberts, R. W. Optimized synthesis of RNA–protein fusions for *in vitro* protein selection. *Methods Enzymol.* **318,** 268–293 (2000).
10. Keefe, A. D. in *Current Protocols in Molecular Biology* (eds Ausubel, F. M. *et al.*) Unit 24.5 (Wiley, New York, 2001).
11. Cadwell, R. C. & Joyce, G. F. Randomization of genes by PCR mutagenesis. *PCR Methods Appl.* **2,** 28–33 (1992).
12. Wilson, D. S. & Keefe, A. D. in *Current Protocols in Molecular Biology* (eds Ausubel, F. M. *et al.*) Unit 8.3 (Wiley, New York, 2000).
13. McCafferty, D. G., Lessard, I. A. D. & Walsh, C. T. Mutational analysis of potential zinc-binding residues in the active site of the enterococcal D-Ala-D-Ala dipeptidase VanX. *Biochemistry* **36,** 10498–10505 (1997).
14. Jenison, R. D., Gill, S. C., Pardi, A. & Polisky, B. High resolution molecular discrimination by RNA. *Science* **263,** 1425–1429 (1994).
15. Wang, Y. & von Hippel, P. H. *Escherichia coli* transcription termination factor Rho. *J. Biol. Chem.* **268,** 13947–13955 (1993).

Supplementary information is available on *Nature*'s World-Wide Web site (http://www.nature.com) or as paper copy from the London editorial office of *Nature*.

Acknowledgements

We thank members of the Szostak laboratory and especially D. Wilson, G. Cho, G. Short, J. Pollard, G. Zimmermann, R. Liu, J. Urbach and R. Larralde-Ridaura for their helpful advice. This work was supported in part by the NASA Astrobiology Institute and the NIH. J.W.S. is an investigator at the Howard Hughes Medical Institute.

Correspondence and requests for materials should be addressed to J.W.S. (e-mail: szostak@molbio.mgh.harvard.edu). The DNA sequences encoding the consensus protein sequences of families A, B, C, D, 18predom and clone 18-19 have been deposited in GenBank under accession codes AF306524 to AF306529, respectively.

correction

The limits of selection during maize domestication

Rong-Lin Wang, Adrian Stec, Jody Hey, Lewis Lukens & John Doebley

Nature **398,** 236–239 (1999)

The primers used for PCR of the 3′ portion of *tb1* amplified a duplicate locus (*tb1* homeologue) in two samples (11 and 16). Inclusion of these homeologous sequences caused π to rise sharply at the 3′ end of the gene in Fig. 1. Using a new 3′ primer (gaggcatcatccagcagacgagaaa), *tb1* sequences were re-isolated (Genbank accessions AF340187–AF340209). The redrawn figure (below) still shows π rising on average, but not as sharply. Because of the known problems with PCR, all statistical tests in the paper were based on sequences isolated as λ clones, and the PCR-isolated sequences were used only in Fig. 1. Thus, other than Fig. 1, no statements or conclusions need amendment. An HKA test with the newly isolated 3′ sequences shows no deviation from neutral expectations for maize ($\chi^2 = 0.49$, $P = 0.78$), and $\pi(\times 1,000)$ for these sequences is 6.7 for teosinte and 5.8 for maize, confirming that selection is not apparent in the 3′ region of *tb1*. □

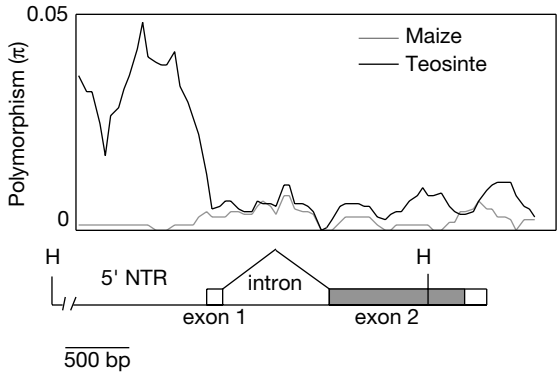

erratum

Scabrous complexes with Notch to mediate boundary formation

Patricia A. Powell, Cedric Wesley, Susan Spencer & Ross L. Cagan

Nature **409,** 626–630 (2000).

The wrong symbol was placed next to Cedric Wesley's name in the author list. He is not presently at the National Science Foundation, but contributed equally to the work with Patricia A. Powell. □

6. Hughen, K., Overpeck, J. T., Peterson, L. C. & Anderson, R. F. in *Palaeoclimatology and Palaeoceanography from Laminated Sediments* (ed. Kemp, A. E. S.) 171–183 (Spec. Publ. 116, Geol. Soc. London, 1996).
7. Adams, J. Paleoseismicity of the Cascadia subduction zone: evidence from turbidites off the Oregon-Washington margin. *Tectonics* **9,** 569–583 (1990).
8. Doig, R. 2300 yr history of seismicity from silting events in Lake Tadiussac, Quebec. *Geology* **18,** 820–823 (1990).
9. Spinrad, R. W. A calibration diagram of specific beam attenuation. *J. Geophys. Res.* **91,** 7761–7764 (1986).
10. Wakeham, S. G. & Ertel, J. R. Diagenesis of organic matter in suspended particles and sediments in the Cariaco Trench. *Org. Geochem.* **13,** 815–822 (1987).
11. Wakeham, S. G. Reduction of stenols to stanols in particulate matter at oxic-anoxic boundaries in sea water. *Nature* **342,** 787–790 (1989).
12. Biscaye, P. E. & Eittreim, S. L. Suspended particulate loads and transports in the nepheloid layer of the abyssal Atlantic Ocean. *Mar. Geol.* **23,** 155–172 (1977).
13. US Geological Survey, National Earthquake Information Center (cited 25 May 1998) ⟨http://www.neic.cr.usgs.gov/⟩.

Acknowledgements. We thank the crew of the RV *Hermano Gines* for their assistance at sea, and W. Gardner, B. Kneller and R. Russo for comments that substantially improved the manuscript. This work was supported by the US NSF and the Venezuelan CONICIT.

Correspondence and requests for materials should be addressed to R.T. (e-mail: thunell@geol.sc.edu).

The limits of selection during maize domestication

Rong-Lin Wang*, Adrian Stec*, Jody Hey†, Lewis Lukens* & John Doebley*

* *Department of Plant Biology, University of Minnesota, St Paul, Minnesota 55108, USA*
† *Department of Genetics, Rutgers University, Piscataway, New Jersey 08854-8082, USA*

The domestication of all major crop plants occurred during a brief period in human history about 10,000 years ago[1]. During this time, ancient agriculturalists selected seed of preferred forms and culled out seed of undesirable types to produce each subsequent generation. Consequently, favoured alleles at genes controlling traits of interest increased in frequency, ultimately reaching fixation. When selection is strong, domestication has the potential to drastically reduce genetic diversity in a crop. To understand the impact of selection during maize domestication, we examined nucleotide polymorphism in *teosinte branched1*, a gene involved in maize evolution[2]. Here we show that the effects of selection were limited to the gene's regulatory region and cannot be detected in the protein-coding region. Although selection was apparently strong, high rates of recombination and a prolonged domestication period probably limited its effects. Our results help to explain why maize is such a variable crop. They also suggest that maize domestication required hundreds of years, and confirm previous evidence that maize was domesticated from Balsas teosinte of southwestern Mexico.

Several lines of evidence indicate that maize is a domesticated form of the wild Mexican grass teosinte (*Zea mays* ssp. *parviglumis* or spp. *mexicana*)[3–5]. Archaeological evidence places the time of maize domestication between 5,000 and 10,000 BP[6]. Despite the recent derivation of maize from teosinte, these plants differ profoundly in morphology[5]. One major difference is that teosinte typically has long branches with tassels at their tips whereas maize possesses short branches tipped by ears. Genetic analyses have identified *teosinte branched1* (*tb1*) as the gene that largely controls this difference[2]. Recent cloning of *tb1* (ref. 7) provides the first opportunity to examine the effects of selection on a 'domestication gene' and to infer from these effects the nature of the domestication process.

During development, *tb1* acts as a repressor of organ growth in those organs in which its messenger RNA accumulates. Consistent with this interpretation, plants carrying the maize allele accumulate more *tb1* mRNA in lateral-branch primordia and have shorter branches (that is, greater repression of branch elongation) than plants carrying the teosinte allele, which accumulate less *tb1* mRNA and have longer branches[7]. This difference in message accumulation between the maize and teosinte alleles suggests that the evolutionary switch from teosinte to maize involved changes in the regulatory regions of *tb1*.

Domestication should strongly reduce sequence diversity at genes controlling traits of human interest. To test this expectation for *tb1*, we sampled a 2.9-kilobase (kb) region (Fig. 1) including most of the predicted transcriptional unit (TU) and 1.1 kb of the 5′ non-transcribed region (NTR) from a diverse sample of maize and teosinte (Table 1). Two measures of genetic diversity were calculated: π, the expected heterozygosity per nucleotide site, and $\hat{\theta}$, an estimate of $4N_e\mu$, where N_e is the effective population size and μ the mutation rate per nucleotide[8]. Within the TU, maize possesses 39% of the diversity found in teosinte, which is not significantly lower than that (71%) seen for the neutral gene, *Adh1* (Table 2). However, within the NTR, maize possesses only 3% of the diversity found in teosinte. Thus, selection during domestication is associated with strongly reduced diversity in the NTR where regulatory sequences are typically found, but more modestly reduced diversity in the TU.

If *tb1* contributed to the morphological evolution of maize, then in the *tb1* phylogeny for maize and teosinte, maize sequences should form a single clade with only minor differentiation among them. Moreover, the type of teosinte most closely related to the direct ancestor of maize should be associated with the maize clade. In contrast, previous research with neutral genes not involved in maize evolution has shown that maize sequences for such genes are dispersed among multiple clades owing to the effects of lineage sorting[9–13]. A phylogeny for the *tb1* TU fits the expectation of a neutral gene, with maize sequences falling into multiple clades (Fig. 2a). However, the phylogeny for the NTR shows all maize on a single, well-supported clade (I) (Fig. 2b), as predicted for a gene involved in maize evolution. There are five teosinte sequences

Table 1 List of taxa and collections sampled

Taxon	Sample	Collection	Origin
MAIZE	**1L**, 1P	BOV396	Bolivia
	2L, 2P	ECU969	Ecuador
	3L, 3P	GUA131	Guatemala
	4L	JAL78	Mexico
	5P	JAL44	Mexico
	6L	MEX7	Mexico
	7L	MOR17	Mexico
	8L	PI213778	North Dakota
	9L	PI218177	Arizona
	10L	SIN2	Mexico
	11L	YUC7B	Mexico
	12L, 12P	VEN604	Venezuela
	13L	W22	Wisconsin
PAR	**14L**, **15L**	BK2	Chilpancingo, Guerrero
	16L, **17L**	BK4	Palo Blanco, Guerrero
	18L	K71-4	Palo Blanco, Guerrero
	19L-A, **B**	B4	Teloloapan, Guerrero
	20P	BK6	Valle de Bravo, Mexico
	21P	IN1480	Jirosto, Jalisco
	22P	IC308	Tzitzio, Michoacan
	23P	BK1	Mazatlan, Guerrero
	24P	Z967	El Rodeo, Jalisco
MEX	**25L**	I28620	Texcoco, Mexico
	26L-A, **B**	B2438	Nobogame, Chihuahua
	27P	D625	Durango, Durango
	28P	D642	Tlamanalco, Mexico
	29P	D479	Texcoco, Mexico
	30P	P11066	Degollado, Jalisco
	31P	W45461	Panindicuaro, Michoacan
	32P	J110	Toluca, Mexico
DIP	**33L**	G1120	Las Joyas, Jalisco

Taxa include *Zea mays* ssp. *mays* (MAIZE), ssp. *parviglumis* (PAR) and ssp. *mexicana* (MEX) and *Zea diploperennis* (DIP). Sequences isolated by λ cloning (L) and PCR (P). Samples for which we isolated and sequenced the 3′ end of the gene are shown in bold. Source of the teosinte collections include G. Beadle (B), B. Benz (Z), T. Cochrane (C), J. Doebley (D), R. Guzman (G), H. Iltis (I), T. A. Kato (K), J. Kermicle (J), M. Nee (N), L. Puga (P) and H. G. Wilkes (W).

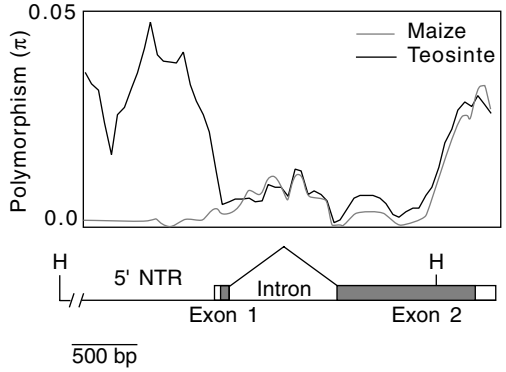

Figure 1 Predicted structure of *teosinte branched1* (ref. 25) and sliding-window analysis of polymorphism (π) in maize and teosinte. For the sliding-window analysis, π was calculated for segments of 300 bp at 50-bp intervals. Sequences used in the analysis were the subset of the λ-cloned sequences for which we isolated the 3′ end by PCR (Table 1). The position of the *Hin*dIII (H) restriction endonuclease sites used in λ cloning are shown, as are the predicted exons (rectangles) and coding region (stippled).

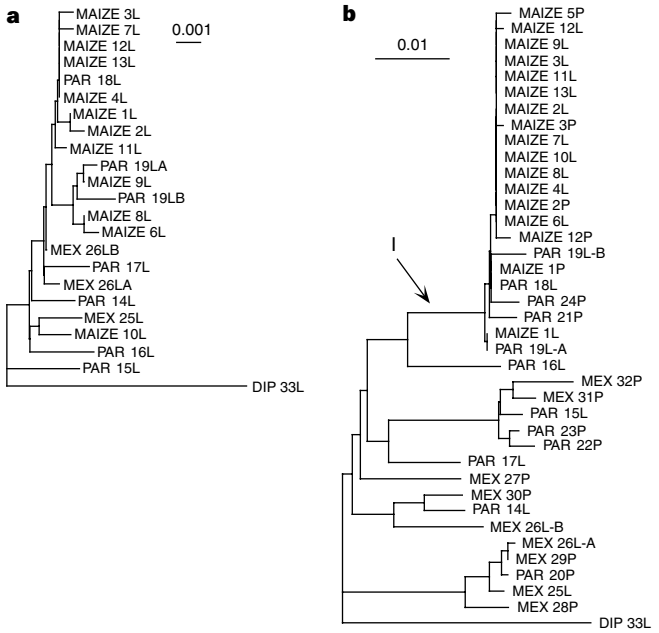

Figure 2 Neighbour-joining trees for *tb1* based on the 1,729-bp transcribed region (**a**) and the 1,143-bp 5′ non-transcribed region (**b**). Taxa include maize, ssp. *parviglumis* (PAR), ssp. *mexicana* (MEX) and the outgroup *Z. diploperennis* (DIP). Sample numbers follow the taxon names. Scale bars indicate the number of substitutions per site using Kimura's 2-parameter distances. Clade I was supported in 200 of 200 bootstrap resamplings of the original data. An initial analysis of the 5′ non-transcribed region using the 22 maize and teosinte λ-cloned sequences indicated that all maize alleles were derived from ssp. *parviglumis*. To confirm whether this result would be sustained with a larger sample, we isolated 16 additional sequences for a more comprehensive analysis (see Methods).

tightly associated with the maize sequences and all belong to ssp. *parviglumis*. The teosinte (sample 16L) basal to clade I also belongs to ssp. *parviglumis*. This phylogeny and previous research[14] provide compelling evidence that ssp. *parviglumis* (Balsas teosinte) is the progenitor of maize and suggest that maize arose in the Balsas river valley of southwestern Mexico, where this subspecies is native.

Although the phylogenies and the relative amount of nucleotide variation in maize suggest that selection has acted on *tb1*, we collected data on nucleotide polymorphism specifically to determine whether *tb1* has experienced a recent selective sweep. This determination was made using the HKA test[15], in which the ratio of polymorphism within a species (maize) to divergence from an outgroup (*Z. diploperennis*) for *tb1* was compared with this ratio for neutral genes. A recent selective sweep in maize would be expected to reduce this ratio for *tb1* relative to neutral genes. The HKA test was not significant for the TU, indicating that there is no evidence for selection on the coding region (Table 3). However, the test was highly significant for the NTR, indicating that selection has strongly reduced variation here. Remarkably, the HKA test for the NTR was significant even if the TU was used as the control. This shows that the 'hitchhiking' effect was so small that it did not even affect the entire gene.

The relative impact of selection on the NTR and TU can be readily seen in a plot of polymorphism (π) for maize and teosinte along the length of *tb1* (Fig. 1). Throughout the NTR, π is substantially lower in maize than in teosinte, reflecting the impact of selection. At the boundary between the NTR and the TU, π for teosinte drops precipitously, as expected, because there is greater constraint on coding regions; however, π for maize rises until it is nearly equal to π for teosinte. Finally, approaching the stop codon at the 3′ end of the gene, π rises steeply in both maize and teosinte, reflecting reduced constraint in this non-translated region. Figure 1 shows graphically how the impact of selection on polymorphism was narrowly focused on the NTR.

As further evidence that regulatory changes in the NTR rather than changes in protein function were involved in maize evolution, we examined the predicted amino-acid sequence of our maize and teosinte sequences. Because our maize and teosinte λ clones did not include the 3′ end of the TU unit, we isolated and sequenced an additional segment spanning the end of the λ clones to ~170 base pairs (bp) downstream of the stop codon (Table 1). Over the entire coding region, there are no fixed differences in the predicted amino-acid sequences between maize and teosinte.

Our analysis of nucleotide polymorphism in *tb1* provides compelling evidence that selection during maize domestication was aimed at the NTR, where regulatory elements are typically found. We had previously observed that the *tb1* mRNA for the maize allele accumulates at twice the level of that for the teosinte allele and proposed that changes in *tb1* regulation underlie maize evolution[7]. Combined evidence from polymorphism analysis and previous work on *tb1* mRNA levels are thus congruent, providing strong evidence that the short, ear-tipped lateral branches of maize evolved from the long, tassel-tipped branches of teosinte by human selection for novel regulatory elements in the NTR.

Although our data implicate selection on regulatory sequences during maize evolution, we found no fixed differences between

Table 2 Nucleotide polymorphism ($\pi/\hat{\theta}$) per bp (×1,000) in maize

Locus	MAIZE	MEX PAR	PAR
tb1:NTR	0.47/0.93	33.08/35.52	28.68/32.57
tb1:TU	1.74/2.43	3.90/6.09	4.62/6.26
Adh1 (ref. 9)	15.72/14.13	–	17.38/20.01

Taxa include *Zea mays* ssp. *mays* (MAIZE), ssp. *parviglumis* (PAR) and ssp. *mexicana* (MEX). These values are based on the 12 maize and 10 teosinte sequences that were cloned in λ (see Table 1).

Table 3 HKA test of neutrality at *tb1* in maize

Test locus	*tb1* NTR	*tb1* TU	*tb1* NTR	*adh1* (ref. 9)	*adh2* (ref. 11)
Control loci	*adh1*, *adh2*	*adh1*, *adh2*	*tb1* TU		
Polymorphism	0.93	2.43	0.93	14.13	25.8
Divergence	52.55	12.73	52.55	21.25	23.6
Ratio	0.018	0.19	0.018	0.66	1.09
χ^2	13.58	2.70	8.24		
P	0.001	0.26	0.004		

Polymorphism ($\hat{\theta}$) and divergence (average pairwise differences between maize and *Z. diploperennis*) are reported per base pair (×1,000).

maize and teosinte within the 1.1 kb of NTR that we analysed. In fact, some maize and teosinte sequences (for example, maize 1P and *parviglumis* 18L) are nearly identical within this region, differing by only 1 bp in the length of a poly(A) track. This may indicate either that the selected site lies further upstream or that the differences between maize and teosinte are complex and depend on a group of polymorphisms rather than a single site[16]. Recombination between an upstream selected site and the region we sequenced could explain why maize is not fully separated from teosinte in the phylogeny (Fig. 2b).

Selection intensities during domestication are expected to be high because crop evolution involves dramatic changes in morphology within a short time. Under directional selection, the selection coefficient (s) is measured as the difference in relative fitness of the most fit and least fit genotypes, where fitness is the contribution of a genotype to the next generation. For example, s 0.01 would indicate that 100 maize alleles would be passed to the next generation for every 99 teosinte alleles. A rough estimate of s requires a knowledge of the recombination rate (c, crossovers per bp per generation) and the distance (d) in bp from the selected site over which there has been a substantial reduction in nucleotide variation[17]:

$$d \quad 0.01s/c$$

For maize, recombination rates have been empirically measured for several genes, giving a mean value for c of $\sim 4 \times 10^{-7}$ (refs 18–21). Two observations allow a preliminary estimate of d: first, the substantial reduction in nucleotide variation is restricted to the NTR or promoter and does not extend into the TU, and, second, plant promoters are normally 2 kb or less in size (see Methods). Thus, the selected site is likely to be less than 2 kb from the TU and must be at least 1.1 kb from the TU since it does not appear to lie in the 1.1 kb of NTR that we sequenced. Using these values, s is estimated to be between 0.04 and 0.08. This estimate can be refined in the future by obtaining direct estimates of c in *tb1* and identifying the precise position of the selected site.

When s is known, one can estimate the time (T_f) required to bring the maize allele to fixation[22]. We assume that the initial frequency of the maize allele was $1/2N$, where N is the population size, and that gene action was additive[2]. We considered two population sizes during the time of selection: 1,000, which assumes teosinte was grown like a horticultural crop in gardens, and 100,000, which assumes it was grown like an agriculture crop but still over a limited geographical area. We assume values for s of 0.04 and 0.08 (see above). For these values, T_f ranges from 315 to 1,023 years. Thus, the morphological evolution of maize as controlled by *tb1* could have been rapid, over just several hundred years.

We were surprised that maize remained polymorphic for *tb1*, even within the NTR. To assess whether the observed level of variation at *tb1* in maize is consistent with previous estimates of mutation and recombination rates, population sizes and the time of maize domestication, we carried out coalescent simulations[23]. The simulations included a selective sweep modelled on a range of estimates for T_s (time since the selective sweep) and s (Table 4). To measure the effect of a selective sweep so that it reflects the present context of not knowing the actual site of selection, we measured the longest segment with zero, one or two polymorphic sites. The simulated mean values of these lengths are remarkably close to the observed data. Thus, even for genes under strong selection, domestication need not remove all variation. The ability of maize to remain polymorphic at *tb1* probably reflects high recombination rates over the hundreds of years required to bring the maize allele to fixation such that there was substantial recombination between the allele that initially harboured the selected site and other alleles in the population. By this means, considerable polymorphism was maintained in the coding region in the face of strong selection on the NTR.

Population-genetic analysis of domestication genes can provide a new view of the processes that sculpted the formation of crop species. For *tb1*, such analysis indicates that ancient agriculturalists exerted a strong selective force on *tb1* that has drastically reduced polymorphism in its regulatory region but not in its coding region. This observation is consistent with previous evidence that alterations in the regulation of *tb1* brought about the change from teosinte to maize plant architecture. We also infer that it took at least several hundred years to bring the maize allele of *tb1* to fixation. Finally, these analyses indicate that Balsas teosinte is the ancestor of maize, since all maize alleles sampled show a close and statistically robust phylogenetic association with this teosinte. □

Table 4 Results from coalescent simulations of the effect of the selective sweep during maize domestication on polymorphism in *tb1*

		Mean lengths (bp)			
T_s	s	0 PS	1 PS	2 PS	
5,000	0.04	682.80	796.20	875.60	Pred.
10,000	0.04	566.00	725.80	830.40	Pred.
5,000	0.08	1,068.40	1,233.20	1,329.00	Pred.
10,000	0.08	892.00	1,133.00	1,321.00	Pred.
–	–	440	760	1,035	Obs.

T_s is the time in generations since the end of the selective sweep, and s is the selection coefficient. The predicted (Pred.) and observed (Obs.) mean lengths of segments with zero, one and two polymorphic sites (PS) are shown.

Methods

Gene isolation. All sequences for population-genetic analysis were cloned into λ-ZAP (Stratagene) as *Hin*dIII fragments (Fig. 1). Isolation of the 3′ end of the gene for the sliding-window analysis (Fig. 1) and determination of the complete amino-acid sequence were accomplished by the PCR reaction (primers: TAGTTCATCGTCACACAGCC and CAATAACGCACACC AGGTCC). PCR was performed using PCR Supermix (Life Technologies) with one step of 4 min at 95 °C followed by 30 cycles of 1 min at 95 °C, 1 min at 60 °C and 3 min at 72 °C followed by 10 min at 72 °C. PCR products were cloned using the TOPO TA cloning kit (Invitrogen). Additional sequences of the NTR for phylogenetic analysis (Fig. 2) were isolated by PCR (primers: GCTATTGGCTACAAGTGACC and GGATAATGTGCACCAGGTGT). All sequences were deposited in GenBank (accession nos AF131649 to AF131705).

Statistics. Calculation of the range of reasonable values for s requires an estimate of the position of the selected site relative to the TU. The selected site is expected to lie within the NTR region in which regulatory sequences occur. Such regions typically extend 2 kb or less upstream of the TU in plants. For example, average gene density in *Arabidopsis* is one gene for every 4.8 kb[24]. With an average gene being about 2.5 kb long, this leaves about 2 kb for flanking regulatory sequences. Moreover, many reports in the literature reveal that 5′ regulatory sequences are usually within 1 kb of the transcription start site. For the coalescent simulations, the middle of the 4,000-bp sampled chromosomes was set as the point of a selective sweep. For the moderate values of s modelled, the use of deterministic allele frequency change will closely follow a stochastic selective sweep[17]. The population mutation rate (θ) was set to 0.0262 per bp, which is the estimated value from teosinte in the *tb1* NTR. The effective population size was set to the value (700,000) estimated for maize at *Adh1*, based on estimates of θ and μ for *Adh1* (ref. 9). The recombination rate (c) was set to 4×10^{-7} as described in the text. Sample size was 12, the same as the number of maize λ clones, and 200 runs were performed.

Received 27 November 1998; accepted 1 February 1999.

1. Harlan, J. *Crops and Man* (Am. Soc. Agron., Madison, WI, 1992).
2. Doebley, J., Stec, A. & Gustus, C. *Teosinte branched1* and the origin of maize: evidence for epistasis and the evolution of dominance. *Genetics* **141,** 333–346 (1995).
3. Beadle, G. Teosinte and the origin of maize. *J. Hered.* **30,** 245–247 (1939).
4. Galinat, W. The origin of maize as shown by key morphological traits of its ancestor, teosinte. *Maydica* **28,** 121–138 (1983).
5. Iltis, H. From teosinte to maize: the catastrophic sexual transmutation. *Science* **222,** 886–894 (1983).
6. Smith, B. *The Emergence of Agriculture* (Freeman, New York, 1995).
7. Doebley, J., Stec, A. & Hubbard, L. The evolution of apical dominance in maize. *Nature* **386,** 485–488 (1997).
8. Watterson, G. On the number of segregating sites in genetical models without recombination. *Theor. Popul. Biol.* **7,** 188–193 (1975).
9. Eyre-Walker, A., Gaut, R., Hilton, H., Feldman, D. & Gaut, B. Investigation of the bottleneck leading to the domestication of maize. *Proc. Natl Acad. Sci. USA* **95,** 4441–4446 (1998).
10. Buckler, E. & Holtsford, T. *Zea* systematics: ribosomal ITS evidence. *Mol. Biol. Evol.* **13,** 612–622 (1996).

11. Goloubinoff, P., Paabo, S. & Wilson, A. Evolution of maize inferred from sequence diversity of an *Adh2* gene segment from archaeological specimens. *Proc. Natl Acad. Sci. USA* **90,** 1997–2001 (1993).
12. Hanson, M. *et al.* Evolution of anthocyanin biosynthesis in maize kernels: the role of regulatory and enzymatic loci. *Genetics* **143,** 1395–1407 (1996).
13. Hilton, H. & Gaut, B. Speciation and domestication in maize and its wild relatives. Evidence from the *globulin-1* gene. *Genetics* **150,** 863–872 (1998).
14. Doebley, J., Goodman, M. & Stuber, C. Isoenzymatic variation in *Zea* (Gramineae). *Syst. Bot.* **9,** 203–218 (1984).
15. Hudson, R., Kreitman, M. & Aguade, M. A test of neutral molecular evolution based on nucleotide data. *Genetics* **116,** 153–159 (1987).
16. Stam, L. F. & Laurie, C. C. Molecular dissection of a major gene effect on a quantitative trait: the level of alcohol dehydrogenase expression in *Drosophila melanogaster*. *Genetics* **144,** 1559–1564 (1996).
17. Kaplan, N., Hudson, R. & Langley, C. The "hitchhiking effect" revisited. *Genetics* **123**, 887–899 (1989).
18. Okagaki, R. & Weil, C. Analysis of recombination sites within the maize *waxy* locus. *Genetics* **147,** 815–821 (1997).
19. Patterson, G., Kubo, K., Shroyer, T. & Chandler, V. Sequences required for paramutation of the maize *b* gene map to a region containing the promoter and upstream sequences. *Genetics* **140,** 1389–1406 (1995).
20. Dooner, H. & Martinez-Ferez, I. Recombination occurs uniformly within the *bronze* gene, a meiotic recombination hotspot in the maize genome. *Plant Cell* **9,** 1633–1646 (1997).
21. Xu, X., Hsia, A., Zhang, L., Nikolau, B. & Schnable, P. Meiotic recombination break points resolve at high rates at the 5′ end of a maize coding sequence. *Plant Cell* **7,** 2151–2161 (1995).
22. Kimura, M. & Ohta, T. The average number of generation until fixation of a mutant gene in a finite population. *Genetics* **61,** 763–771 (1969).
23. Hudson, R. Properties of a neutral allele model with intragenic recombination. *Theor. Popul. Biol.* **23,** 183–201 (1983).
24. Bevan, M. *et al.* Analysis of 1.9 Mb of contiguous sequence from chromosome 4 of *Arabidopsis thaliana*. *Nature* **391,** 485–488 (1998).
25. Doebley, J. & Stec, A. The structure of *teosinte branched1*: a progress report. *Maize Genet. Coop. News1.* **73** (1998).

Acknowledgements. We thank E. Buckler, B. Gaut and J. Wendel for comments. This research was supported by the NSF and the Plant Molecular Genetics Institute of the University of Minnesota.

Correspondence and requests for materials should be addressed to J.D. (e-mail: doebley@tc.umn.edu).

Gaze direction controls response gain in primary visual-cortex neurons

Yves Trotter & Simona Celebrini

Centre de Recherche Cerveau et Cognition, Faculté de Médecine de Rangueil, Université Paul Sabatier, 133, route de Narbonne, 31062 Toulouse Cedex, France

To localize objects in space, the brain needs to combine information about the position of the stimulus on the retinae with information about the location of the eyes in their orbits. Interaction between these two types of information occurs in several cortical areas[1–12], but the role of the primary visual cortex (area V1) in this process has remained unclear. Here we show that, for half the cells recorded in area V1 of behaving monkeys, the classically described visual responses are strongly modulated by gaze direction. Specifically, we find that selectivity for horizontal retinal disparity—the difference in the position of a stimulus on each retina which relates to relative object distance—and for stimulus orientation may be present at a given gaze direction, but be absent or poorly expressed at another direction. Shifts in preferred disparity also occurred in several neurons. These neural changes were most often present at the beginning of the visual response, suggesting a feedforward gain control by eye position signals. Cortical neural processes for encoding information about the three-dimensional position of a stimulus in space therefore start as early as area V1.

Area V1 is the first cortical area where orientation and horizontal retinal disparity are encoded[13–15]. Here, cells have oriented receptive fields that may occupy disparate locations on both retinae. Most of these cells have their activity (visual and/or spontaneous) modulated by the viewing distance in the straight-ahead sagittal direction[16,17]. But do such modulations also occur as a function of the direction of gaze? This would imply that V1 cells would be more dedicated to certain volumes of visual space, in which case changing the direction of gaze should affect some or all of the visual properties encoded in the primary visual cortex, such as horizontal retinal disparity and orientation selectivity.

We obtained data from 142 neurons in two monkeys that were trained to fixate a target at three different positions in the frontoparallel plane (Fig. 1a). For studies of both disparity and orientation, changes in gaze direction produced significant changes in neuronal activity in 54% (n 67) of cells tested for disparity and 50% (n 104) tested for orientation. The main effect was a significant change in the evoked firing rate (gain) in 72% of cells studied for disparity and in 85% studied for orientation. Shifts in preferred disparity angle were observed in 17% of cells; the remainder showed inconclusive changes in the tuning curves. Three examples of the gain effect on disparity coding are shown in Fig. 2. The cell shown in Fig. 2a is disparity selective with the preferred response in the plane of fixation (0°) when the monkey fixates in the centre of the screen or on the left, but shows a significant drop in the level of visual response, close to the spontaneous activity level, when the monkey fixates on the right. The cell shown in Fig. 2b exhibits significant progressive increase in the evoked firing rate in the plane of fixation (tuned 0°) from the left to the right direction of gaze. That shown in Fig. 2c displays a shift in preferred disparity angle: it has a preferred disparity angle in the plane of fixation (0°) for a gaze directed to the left, but shifts its peak just behind that plane (centred on 0.2°) for the right direction, with an intermediate step for the straight-ahead direction.

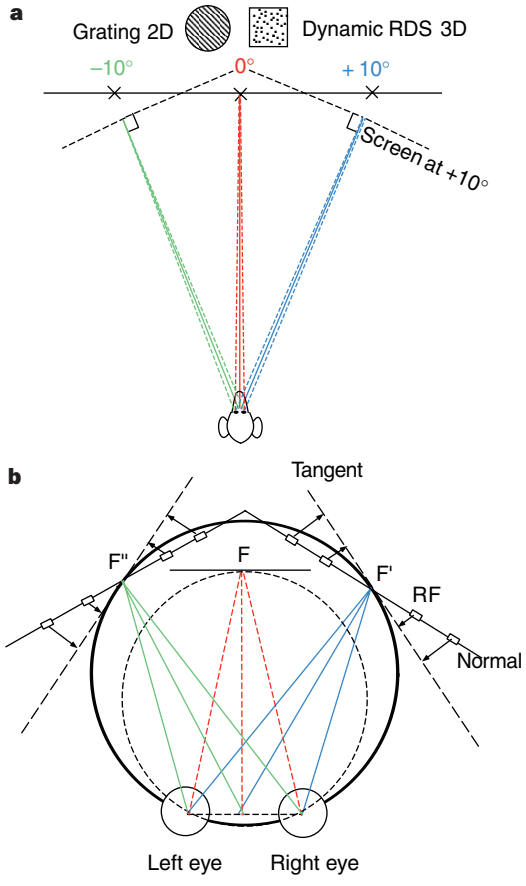

Figure 1 Experimental set-up. **a**, Dynamic random dot stereograms (RDS) and square-wave gratings were flashed on a video monitor screen subtending 42° or 32° of visual angle at three directions of gaze (straight ahead, 0°; left, –10°; and right, +10°) in the frontoparallel plane. For the left and right directions, the video monitor was rotated by 10° to maintain geometrical configurations with the viewing distance kept constant at 50 cm. Continuous lines of view represent the binocular axis. **b**, Vieth–Müller circles passing through both eyes and through fixation point for the three directions of gaze (F, F′ and F″) (adapted from ref. 19).

blotting of gels run in parallel, and Hb(β) and Hb(α) were discriminated by their differential electrophoretic mobility.

Bioassay

Rabbit aortic rings were suspended in Krebs-bicarbonate buffer at 37 °C, bubbled continuously with either 95% O_2/5% CO_2 or 95% argon/5% CO_2 (measured O_2 less than 1%)[1,2]. Resting tension was maintained at a standard 2 g and active tension was induced by phenylephrine. NO-treated and control RBCs were washed and resuspended in PBS at 50% haematocrit, and added to individual 25-ml baths as 0.2-ml aliquots to yield a bath haematocrit of 0.4%. RBCs were treated with AE1 inhibitors (DIDS, niflumic acid or phenylglyoxal; 0.1 mM in all cases) for 60 min before washing and exposure to NO.

Received 20 April; accepted 6 November 2000.

1. Jia, L., Bonaventura, C., Bonaventura, J. & Stamler, J. S. *S*-nitrosohaemoglobin: a dynamic activity of blood involved in vascular control. *Nature* **380,** 221–226 (1996).
2. Stamler, J. S. *et al.* Blood flow regulation by *S*-nitrosohemoglobin is controlled by the physiological oxygen gradient. *Science* **276,** 2034–2037 (1997).
3. Gow, A. J. & Stamler, J. S. Reactions between nitric oxide and haemoglobin under physiological conditions. *Nature* **391,** 169–173 (1998).
4. Gow, A. J., Luchsinger, B. P., Pawloski, J. R., Singel, D. J. & Stamler, J. S. The oxyhemoglobin reaction of nitric oxide. *Proc. Natl Acad. Sci. USA* **96,** 9027–9032 (1999).
5. McMahon, T. J., Stone, A. E., Bonaventura, J., Singel, D. J. & Stamler, J. S. Functional coupling of oxygen-binding and vasoactivity in *S*-nitrosohemoglobin. *J. Biol. Chem.* **275,** 16738–16745 (2000).
6. McMahon, T. J. & Stamler, J. S. Concerted nitric oxide/oxygen delivery by hemoglobin. *Methods Enzymol.* **301,** 99–114 (1999).
7. Pawloski, J. R., Swaminathan, R. V. & Stamler, J. S. Cell-free and erythrocytic *S*-nitrosohemoglobin inhibits human platelet aggregation. *Circulation* **97,** 263–267 (1998).
8. Rauenbuehler, P. B., Cordes, K. A. & Salhany, J. M. Identification of the hemoglobin binding sites on the inner surface of the erythrocyte membrane. *Biochim. Biophys. Acta* **692,** 361–370 (1982).
9. Walder, J. A. *et al.* The interaction of hemoglobin with the cytoplasmic domain of band 3 of the human erythrocyte membrane. *J. Biol. Chem.* **259,** 10238–10246 (1984).
10. Low, P. S. Structure and function of the cytoplasmic domain of band 3: center of erythrocyte membrane–peripheral protein interactions. *Biochim. Biophys. Acta* **864,** 145–167 (1986).
11. Kondo, T. Preparation of microcapsules from human erythrocytes: use in transport experiments of glutathione and its S-conjugate. *Methods Enzymol.* **171,** 217–225 (1989).
12. Stamler, J. S., Toone, E. J., Lipton, S. A. & Sucher, N. J. (S)NO signals: translocation, regulation, and a consensus motif. *Neuron* **18,** 691–696 (1997).
13. Sayare, M. & Fikiet, M. Cross-linking of hemoglobin to the cytoplasmic surface of human erythrocyte membranes. Identification of band 3 as a site for hemoglobin binding in Cu^{2+}-*o*-phenanthroline catalyzed cross-linking. *J. Biol. Chem.* **256,** 13152–13158 (1981).
14. Liu, S. Q. & Knauf, P. A. Lys-430, site of irreversible inhibition of band 3 Cl^- flux by eosin-5-maleimide, is not at the transport site. *Am. J. Physiol.* **264,** C1155–C1164 (1993).
15. Falke, J. J. & Chan, S. I. Molecular mechanisms of band 3 inhibitors. 1. Transport site inhibitors. *Biochemistry* **25,** 7888–7894 (1986).
16. Okubo, K., Kang, D., Hamasaki, N. & Jennings, M. L. Red blood cell band 3. Lysine 539 and lysine 851 react with the same H2DIDS (4,4′-diisothiocyanodihydrostilbene-2,2′-disulfonic acid) molecule. *J. Biol. Chem.* **269,** 1918–1926 (1994).
17. Salhany, J. M., Cordes, K. A. & Gaines, E. D. Light-scattering measurements of hemoglobin binding to the erythrocyte membrane. Evidence for transmembrane effects related to a disulfonic stilbene binding to band 3. *Biochemistry* **19,** 1447–1454 (1980).
18. Hsu, L. & Morrison, M. The interaction of human erythrocyte band 3 with cytoskeletal proteins. *Archiv. Biochem. Biophys.* **227,** 31–38 (1983).
19. Macara, I. G., Kuo, S. & Cantley, L. C. Evidence that inhibitors of anion exchange induce a transmembrane conformational change in band 3. *J. Biol. Chem.* **258,** 1785–1792 (1983).
20. Falke, J. J. & Chan, S. I. Molecular mechanisms of band 3 inhibitors. 3. Translocation inhibitors. *Biochemistry* **25,** 7899–7906 (1986).
21. Chetrite, G. & Cassoly, R. Affinity of hemoglobin for the cytoplasmic fragment of human erythrocyte membrane band 3. Eqilibrium measurements at physiological pH using matrix-bound proteins: the effects of ionic strength, deoxygenation and of 2,3,-diphosphoglycerate. *J. Mol. Biol.* **185,** 639–644 (1985).
22. Galanter, W. L. & Labotka, R. J. The binding of nitrate to the human anion exchange protein (AE1) studied with ^{14}C nuclear magnetic resonance. *Biochim. Biophys. Acta* **1079,** 146–151 (1991).
23. Shingles, R., Roh, M. H. & McCarty, R. E. Direct measurement of nitrite transport across erythrocyte membrane vesicles using the fluorescent probe, 6-methoxy-*N*-(3-sulfopropyl) quinolinium. *J. Bioenerg. Biomembr.* **29,** 611–616 (1997).
24. Soszynski, M. & Bartosz, G. Penetration of erythrocyte membrane by peroxynitrite: participation of the anion exchange protein. *Biochem. Mol. Biol. Int.* **43,** 319–325 (1997).
25. Czerwinski, M. *et al.* Degradation of the human erythrocyte membrane band 3 studied with the monoclonal antibody directed against an epitope on the cytoplasmic fragment of band 3. *Eur. J. Biochem.* **174,** 647–654 (1988).
26. Telen, M. J., Scearce, R. M. & Haynes, B. Human erythrocyte antigens. III. Characterization of a panel of murine monoclonal antibodies that react with human erythrocyte and erythroid precursor membranes. *Vox Sang.* **52,** 236–243 (1987).
27. Liu, X. *et al.* Diffusion-limited reaction of free nitric oxide with erythrocytes. *J. Biol. Chem.* **273,** 18709–18713 (1998).
28. Vaughn, M. W., Huang, K.-T., Kuo, L. & Liao, J. C. Erythrocytes possess an intrinsic barrier to nitric oxide consumption. *J. Biol. Chem.* **275,** 2342–2348 (2000).

Acknowledgements

We are grateful to M. Telen for providing antibody to AE1 and for advice. This work was supported by an AHA postdoctoral fellowship to J.R.P.

Correspondence and requests for materials should be addressed to J.S.S. (e-mail: STAML001@mc.duke.edu).

Scabrous complexes with Notch to mediate boundary formation

Patricia A. Powell*†‡, Cedric Wesley§‡, Susan Spencer* & Ross L. Cagan*

* *Department of Molecular Biology and Pharmacology, Washington University School of Medicine, 660 South Euclid Avenue, Campus Box 8103, St. Louis, Missouri 63110, USA*
§ *Laboratory of Genetics, The Rockefeller University, 1230 York Avenue, York, New York 10021, USA*
† *These authors contributed equally to this work*

The mechanisms that establish and sharpen pattern across epithelia are poorly understood. In the developing nervous system, the first pattern elements appear as 'proneural clusters'. In the morphogenetic furrow of the immature *Drosophila* retina proneural clusters emerge in a wave as a patterned array of 6–10-cell groups, which are recognizable by expression of Atonal, a basic helix–loop–helix transcription factor that is required to establish and pattern the first cell fate[1–3]. The establishment and subsequent patterning of Atonal expression requires activity of the signalling transmembrane receptor Notch[2,4]. Here we present *in vivo* and biochemical evidence that the secreted protein Scabrous associates with Notch, and can stabilize Notch protein at the surface. The result is a regulation of *Notch* activity that sharpens proneural cluster boundaries and ensures establishment of single pioneer neurons.

In the morphogenetic furrow, Atonal's expression can be divided into four steps[1–3] (Fig. 1a). First, it is expressed as a broad, unpatterned stripe; second, expression is then upregulated into evenly spaced proneural clusters; third, in these proneural clusters, a 2–3-cell 'R8 equivalence group' emerges; and last, expression narrows to identify a single cell in this group as the R8 photoreceptor neuron, the first cell type of the developing retina. In each step, as cells lose Atonal expression they concurrently gain expression of negative regulators, such as members of the E(spl) (Enhancer of Split) complex[1,2] (Fig. 1a). Expression of E(spl) initially requires the presence of Atonal[3], and is subsequently amplified by the *Notch* signalling pathway to downregulate proneural bHLH expression and function[4,5]. E(spl), therefore, represents one reporter of *Notch* activity.

Patterning of Atonal and E(spl) expression requires normal activity of Scabrous, a secreted fibrinogen-related protein with a potential for association with components of the extracellular matrix[6–8]. In the retina, Scabrous protein first appears in the proneural clusters, mirroring Atonal expression by narrowing to the R8 equivalence group, and eventually R8 alone. This expression is dependent on Atonal activity[9], which indicates that the *scabrous* locus may be a direct target of Atonal.

Genotypically null sca^{BP2} proneural clusters are poorly spaced with poorly defined borders (Fig. 1b)[10,11]. Broadened E(spl) expression throughout much of the proneural cluster region is one potential cause of this imprecision (Fig. 1b), suggesting that Notch activity is altered in sca^{BP2} mutants. These observations suggest that initial broad, low-level Atonal expression activates broad, low-level E(spl) expression, and that Scabrous is required to refine the complementary Atonal and E(spl) expression in the proneural cluster region—events also associated with *Notch* activity.

A 1-h pulse of ectopic Scabrous resulted in rapid loss of Atonal within 2 h (Fig. 1d); E(spl) showed low, diffuse expression (Fig. 1d) that was lost within 4 h (data not shown). This ectopic expression of

‡ Present address: National Science Foundation, 4201 Wilson Blvd., Arlington, Virginia 22230, USA.

Scabrous leads to aberrant patterning of R8s in a manner similar to that of the phenotypes observed in *scabrous* loss-of-function alleles[11]. Corresponding wild-type heat shock had no effect (data not shown). The loss of the initial broad stripe of Atonal, a *Notch*-dependent step[12], suggests that ectopic Scabrous can lead to a disruption of *Notch* function, a result consistent with overexpression studies in the *Drosophila* wing[13].

Subsequent resolution of Atonal expression in the equivalence group, also a *Notch*-dependent step[10,14,15], is delayed in sca^{BP2} mutants (Fig. 1b). Delay of Atonal resolution can result in ectopic R8s (ref. 1); indeed, 40% of sca^{BP2} ommatidia ($n = 200$) contain two or three R8s derived from the R8 equivalence group (Fig. 1c). R8s were observed to be both adjacent and non-adjacent, indicating that selection may be stochastic.

These results suggest that Scabrous influences the establishment or maintenance of boundaries of *Notch* activity during both proneural-cluster and R8 equivalence-group maturation. To investigate the nature of this influence, transient expression of full-length Notch protein (N350) in *Drosophila* S2 tissue-culture cells was examined by western analysis (Fig. 2a; $n = 14$ experiments). Transiently induced N350 was depleted gradually over 7 h; this loss was accelerated in the presence of Delta (Fig. 2a). In contrast, addition of Scabrous led to an accumulation of N350 and smaller Notch fragments, even in the presence of Delta (Fig. 2a). Accumulation of Notch was not due to induction of the endogenous *Notch* gene, which is rearranged in S2 cells (ref. 16; and C.S.W., unpublished observations). Cell-surface biotinylation analysis indicated that the presence of Scabrous significantly stabilized N350 at the cell surface (Fig. 2b); however, the functional nature of this stabilization remains unknown.

Genetic and histological studies have suggested a function for Scabrous as a secreted Notch ligand[10,17]. However, attempts to show this interaction biochemically have been unsuccessful[18]. We returned to this issue using two independent assays. Notch is expressed throughout embryogenesis[19,20], whereas Scabrous protein was detected in young (2.5–6.5 h) but not more mature (12.5–16.5 h) embryos (Fig. 2c). Immunoprecipitation with a mouse polyclonal anti-Scabrous antibody led to a complex with a relative molecular mass of 300,000 (M_r 300K) that contained both Scabrous and Notch protein (Fig. 2c). The size and composition of the 300K complex indicates that it may include a truncated form of Notch previously characterized *in vivo*[21]. As controls, crosslinked complexes recovered by an anti-Delta antibody included Notch, but complexes recovered by an anti-Fasciclin III antibody did not (data not shown).

To investigate binding *in vivo*, we used the fact that diffusible ligands can be stabilized specifically in cells expressing their natural receptor[22]. In the midpupal eye, Notch is expressed exclusively in a set of interommatidial cells, the secondary and tertiary pigment cells (Fig. 3a)[20]. Scabrous is not expressed in the retina at this developmental stage (Fig. 3b). Transient heat-shock induction of *hs-scabrous* pupae resulted in a ubiquitous pulse of Scabrous protein

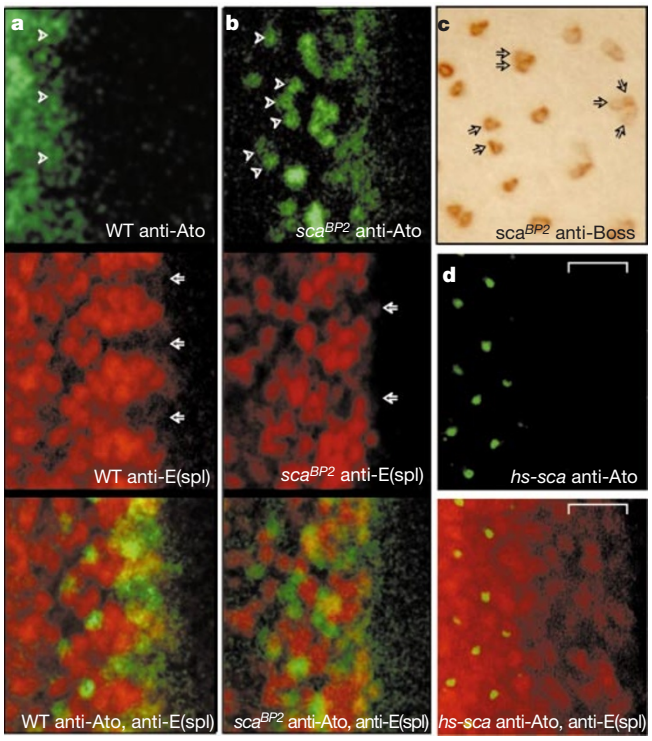

Figure 1 Altering Scabrous activity. Anterior is toward the right. **a**, Atonal and E(spl) expression in wild-type (WT) morphogenetic furrow. Top, Atonal expression evolves from low and diffuse to high in regularly spaced proneural clusters and eventually R8s (arrowheads). Middle, E(spl) (mδ, mγ, mβ and m3) extends between, but not in (arrows), proneural clusters. **b**, Atonal and E(spl) expression in sca^{BP2} morphogenetic furrow. Top, Atonal expression is low and diffuse; proneural clusters are shorter with poorly delineated boundaries. Expression is later retained in 2–3 cells (arrowheads). Middle, E(spl) extends into proneural cluster regions (arrows). Poorly spaced sca^{BP2} ommatidia often contain several R8s (marked with Boss; arrows) (**c**). **d**, Effect of ectopic Scabrous (*hs-scabrous*) on Atonal and E(spl) expression. Top, *hs-scabrous* blocks Atonal espression in morphogenetic furrow (bracket). R8s are labelled with Boss. Bottom, E(spl) is unpatterned and diffuse.

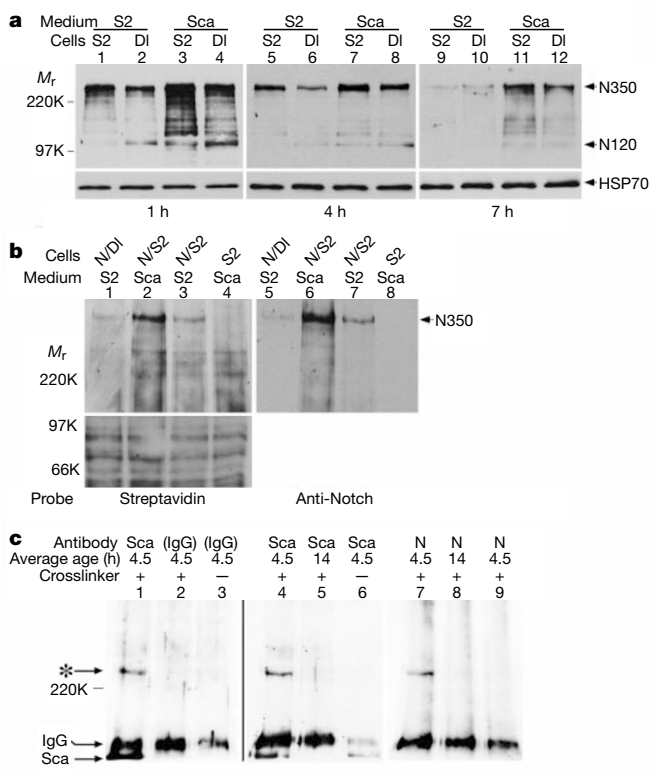

Figure 2 Scabrous stabilizes Notch and forms a complex *in vivo*. **a**, Western analysis of S2 tissue-culture cells. S2-Notch cells treated with Scabrous for 1, 4 or 7 h have higher N350 levels even in presence of Delta. N120 is a Notch intracellular fragment. Conditioned media: S2, S2-hsSca. Cell lines: S2, S2-Notch, S2-Dl. **b**, Cell-surface biotinylation analysis. More N350 molecules are biotinylated in the presence of Scabrous. Other cell-surface molecules are biotinylated at similar levels (below lanes 1–4). Lanes 5–8 are the same as lanes 1–4, but reprobed with Notch antibody to detect N350. **c**, Scabrous antibody immunoprecipitates ~300K complex (asterisk) containing Scabrous and Notch (lanes 1, 4, 7) during stages of high Scabrous expression (lanes 4, 5).

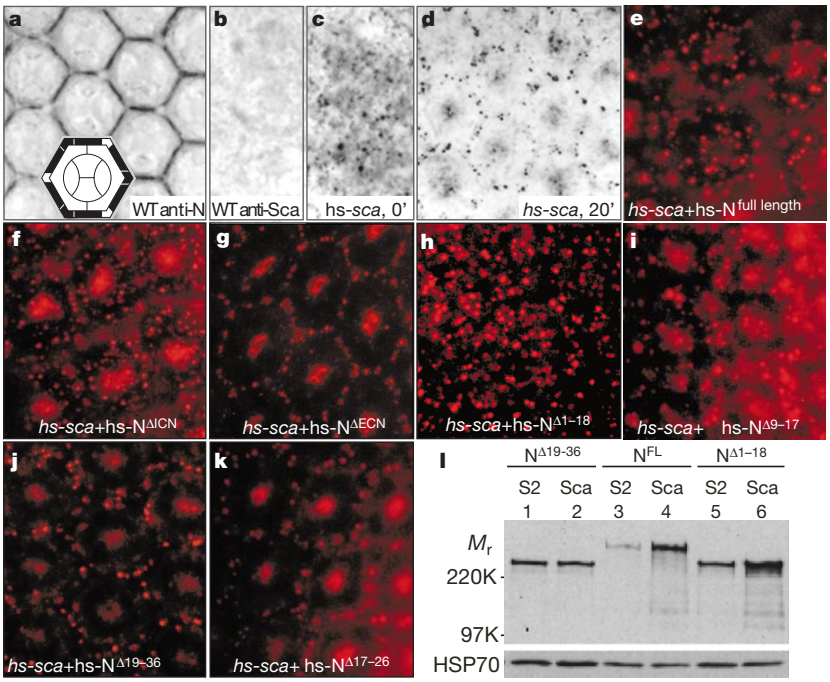

Figure 3 Scabrous and Notch collocalize *in vivo*. Apical surface of 38-h pupal retinae. **a**, Notch expression in interommatidial cells. Notch is expressed exclusively in secondary/tertiary pigment cells (shaded; inset). **b**, Scabrous is not expressed. Shifting *hs-scabrous* pupae to 37 °C results in broad Scabrous expression (**c**) that is lost 10 min later (**d**) except in secondary/tertiary pigment cells. The strong staining at the ommatidial centre is Scabrous that is trapped in photoreceptor rhabdomeres. Full-length Notch, $N^{\Delta ICN}$, $N^{\Delta 9-17}$ and $N^{\Delta 1-18}$ (**e**, **f**, **h**, **i**), but not $N^{\Delta ECN}$, $N^{\Delta 17-26}$ or $N^{\Delta 19-36}$ (**g**, **j**, **k**), stabilizes Scabrous in all cells. **l**, After 4 h, addition of Scabrous stabilizes full-length Notch and $N^{\Delta 1-18}$, but not $Notch^{\Delta 19-36}$.

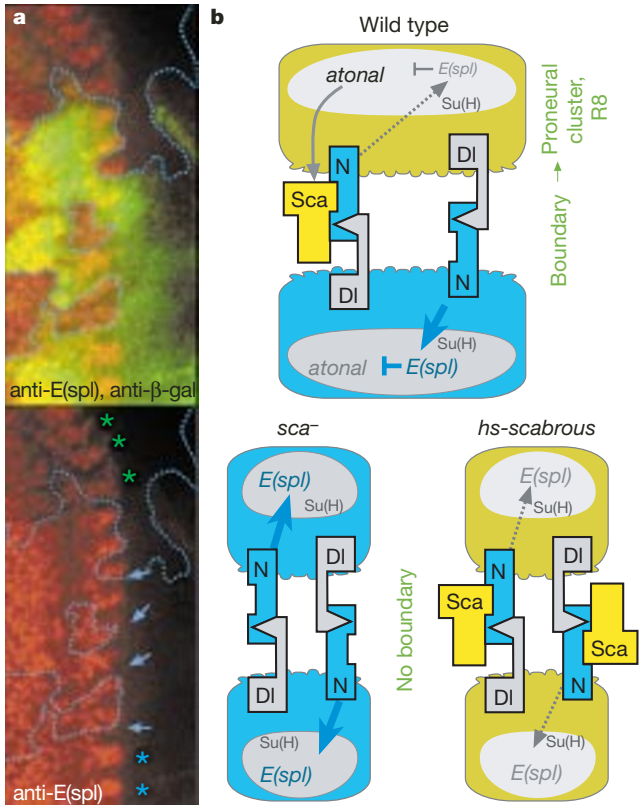

Figure 4 Scabrous and boundaries. **a**, Top, Lack of β-galactosidase expression (cytoplasmic, green) in sca^{BP2} clones (dotted lines). Bottom, Within, but near clone edges (blue arrows), E(spl) expression (nuclear, red) often re-orientates to match clone boundary. Compare with sharp wild-type (blue asterisks) and diffuse, fully sca^{BP2} (green asterisks) boundaries. **b**, Model. Cells expressing high levels of Atonal (proneural cluster, R8 equivalence group) express Scabrous, reducing their *Notch* activity and E(spl) expression (dotted arrow). Neighbouring cells that fail to express Scabrous show high *notch* activity (solid arrow), further reducing Atonal expression. Initial Atonal differences are amplified, stabilizing proneural cluster edges and later ensuring single R8s. Su(H), Suppressor of Hairless.

(Fig. 3c) that was processed, secreted and rapidly lost from most cells in as little as 5 min after the end of heat shock. However, Scabrous was retained in secondary/tertiary cells (Fig. 3d), the same cells that express the Notch receptor. Retention of Scabrous occurred in apically localized vesicles commonly observed with secreted ligands and their receptors, including Notch[23]. This cell-type-specific retention suggests that a receptor for Scabrous is found specifically in the secondary/tertiary cells at this stage of development.

We next altered the expression pattern of Notch through an inducible heat-shock promoter. Co-expression of Scabrous and Notch in all retinal cells resulted in the stabilization of Scabrous in all cells (Fig. 3e). Similarly, ubiquitous expression of an inactive form of Notch that lacked its intracellular domain[24] ($N^{\Delta ICN}$) was also sufficient to stabilize exogenous Scabrous in all cells (Fig. 3f), indicating that Scabrous may associate with the extracellular domain of Notch. This also indicates that stabilization of Scabrous did not require the signalling activity of Notch. As predicted, a membrane-tethered form of the intracellular domain[24] ($N^{\Delta ECN}$) did not retain Scabrous (Fig. 3g).

The extracellular domain of Notch includes 36 epidermal growth factor (EGF)-like repeats. Two demonstrated ligands of Notch, Delta and Serrate, require EGF-like repeats 11 and 12 for binding[25]. Ubiquitous expression of Notch forms that deleted repeats 1–18 or 9–17 ($N^{\Delta 1-18}$ and $N^{\Delta 9-17}$) was still sufficient to stabilize Scabrous protein in all retinal cells (Figs 3h, i); however, $N^{\Delta 19-36}$ and $N^{\Delta 17-26}$ failed to retain Scabrous protein (Figs 3j, k). Western analysis indicated that $N^{\Delta 9-17}$ and $N^{\Delta 17-26}$ were expressed at similar levels in pupal eye discs after heat shock (data not shown). The inability of $N^{\Delta 19-36}$ or $N^{\Delta 17-26}$ to retain Scabrous suggests that the site of Notch/Scabrous association lies within repeats 19–26. Consistent with this view, Scabrous protein was able to promote stabilization of $N^{\Delta 1-18}$ that was expressed on the surface of S2 cells, but failed to stabilize $N^{\Delta 19-36}$ (Fig. 3l).

Our data support the view[10,13,17] that Scabrous and Notch form a receptor–ligand pair; however, we cannot rule out the possibility that binding requires other cofactors or adapters. Our results indicating stabilization suggest that Scabrous may act to scaffold Notch protein to the extracellular matrix and downregulate *Notch* activity in at least some experimental situations[13] to sharpen local boundaries. Consistent with this view, the sharp boundaries between proneural clusters were lost in sca^{BP2} clonal patches (Fig. 4a), indicating that Scabrous may act over a short distance. Notably, when a sca^{BP2} clonal patch crossed the morphogenetic furrow, high E(spl) expression typically coincided with the boundary of the clone (14 out of 18 sca^{BP2} clonal patches adjacent to a proneural cluster followed its boundary, as compared with 5 out of 14 wild-type control clones).

The observed complexity of their *in vivo* interactions leaves the precise mechanism by which Scabrous regulates Notch at boundaries unresolved. One model is presented in Fig. 4b. *Notch* signalling establishes boundaries during a variety of epithelial developmental decisions, and similar to Fringe[26], Scabrous provides a means by which Notch activity can be altered in the absence of changes in ligand expression, although the tissues and possibly the mechanisms, are different. □

Methods

Heat shocks

hs-scabrous larvae received a 1-h heat pulse at 37 °C, and recovered for 1–4 h. For *in vivo* binding, white prepupae were aged at 25 °C for 37 h, then heat shocked at 37 °C for 2 × 12 min with intervening 90 min recovery at 25 °C, held at 25 °C for 20 min, and iced. We then dissected the pupal eyes directly into PLP fixative[1].

Immunohistochemistry

The antibodies used were anti-Atonal (1:10,000)[9], anti-E(spl)323 (1:10)[27], anti-Notch (1:50)[16] and anti-Scabrous (1:10)[10]. We used standard fixation and staining protocols[1]. Confocal images for Fig. 1a and b were captured, and projections created with ImageSpace software (Molecular Dynamics).

Clonal analysis

yw hsFLP;FRT42 conD lacZ/CyO flies were crossed with *FRT42* sca^{BP2}*/Bc Gla* or (as a control) *FRT42* flies. To prevent scoring bias, tracings of the *lacZ* were done in the absence of the E(spl) image. We only scored proneural clusters that lay at least partially outside (but adjacent) to the clones.

Immunoprecipitations

Crosslinked cell surface molecules were immunoprecipitated with a Scabrous antibody[12] and the complexes detected on western blots with the same Scabrous antibody or a Notch antibody[24] as described[21]. We reprobed lanes 4–6 in Fig. 2c to produce lanes 7–9.

Cell culture and western analysis

Heat shocked 10^7 S2 or S2-*hs-scabrous* cells were used to produce 1 ml of conditioned serum-free Shields and Sang M3 medium for treating cells. Cell surfaces were biotinylated for 15 min with 1 mg ml^{-1} Sulpho-NHS-LC-Biotin (Pierce) in HEPES (pH 8.1)-buffered Chan and Gehring medium (Ashburner). Proteins were extracted, quantified and analysed on 4% or 8% SDS-PAGE as described using anti-Notch or streptavidin-conjugated antibodies[21,28,29]. Total protein levels in lanes or samples were assessed using an antibody against HSP 70 (Sigma). Specificity of cell-surface biotinylation was checked by non-biotinylation of the intracellular HSP 70.

Received 22 May; accepted 6 November 2000.

1. Dokucu, M. E., Zipursky, S. L. & Cagan, R. L. Atonal, rough and the resolution of proneural clusters in the developing *Drosophila* retina. *Development* **122,** 4139–4147 (1996).
2. Baker, N. E., Yu, S. & Han, D. Evolution of proneural atonal expression during distinct regulatory phases in the developing *Drosophila* eye. *Curr. Biol.* **6,** 1290–1301 (1996).
3. Jarman, A. P., Sun, Y., Jan, L. Y. & Jan, Y. N. Role of the proneural gene, atonal, in formation of *Drosophila* chordotonal organs and photoreceptors. *Development* **121,** 2019–2030 (1995).
4. Bailey, A. M. & Posakony, J. W. Suppressor of hairless directly activates transcription of enhancer of split complex genes in response to Notch receptor activity. *Genes Dev.* **9,** 2609–2622 (1995).
5. Lecourtois, M. & Schweisguth, F. The neurogenic suppressor of hairless DNA-binding protein mediates the transcriptional activation of the enhancer of split complex genes triggered by Notch signaling. *Genes Dev.* **9,** 2598–2608 (1995).
6. Lee, E. C., Hu, X., Yu, S. Y. & Baker, N. E. The scabrous gene encodes a secreted glycoprotein dimer and regulates proneural development in *Drosophila* eyes. *Mol. Cell. Biol.* **16,** 1179–1188 (1996).
7. Lee, E. C., Yu, S. Y., Hu, X., Mlodzik, M. & Baker, N. E. Functional analysis of the fibrinogen-related scabrous gene from *Drosophila melanogaster* identifies potential effector and stimulatory protein domains. *Genetics* **150,** 663–673 (1998).
8. Mlodzik, M., Baker, N. E. & Rubin, G. M. Isolation and expression of scabrous, a gene regulating neurogenesis in *Drosophila*. *Genes Dev.* **4,** 1848–1861 (1990).
9. Jarman, A. P., Grell, E. H., Ackerman, L., Jan, L. Y. & Jan, Y. N. Atonal is the proneural gene for *Drosophila* photoreceptors. *Nature* **369,** 398–400 (1994).
10. Baker, N. E., Mlodzik, M. & Rubin, G. M. Spacing differentiation in the developing *Drosophila* eye: a fibrinogen-related lateral inhibitor encoded by scabrous. *Science* **250,** 1370–1377 (1990).
11. Ellis, M. C., Weber, U., Wiersdorff, V. & Mlodzik, M. Confrontation of scabrous expressing and non-expressing cells is essential for normal ommatidial spacing in the *Drosophila* eye. *Development* **120,** 1959–1969 (1994).
12. Ligoxygakis, P., Yu, S. Y., Delidakis, C. & Baker, N. E. A subset of Notch functions during *Drosophila* eye development require Su(H) and the E(spl) gene complex. *Development* **125,** 2893–2900 (1998).
13. Lee, E. C., Yu, S. Y. & Baker, N. E. The scabrous protein can act as an extracellular antagonist of Notch signaling in the *Drosophila* wing. *Curr. Biol.* **10,** 931–934 (2000).
14. Cagan, R. L. & Ready, D. F. Notch is required for successive cell decisions in the developing *Drosophila* retina. *Genes Dev.* **3,** 1099–1112 (1989).
15. Baker, N. E. & Zitron, A. E. *Drosophila* eye development: Notch and Delta amplify a neurogenic pattern conferred on the morphogenetic furrow by Scabrous. *Mech. Dev.* **49,** 173–189 (1995).
16. Fehon, R. G. *et al.* Molecular interactions between the protein products of the neurogenic loci Notch and Delta, two EGF-homologous genes in *Drosophila*. *Cell* **61,** 523–534 (1990).
17. Rabinow, L. & Birchler, J. A. Interactions of vestigial and scabrous with the Notch locus of *Drosophila melanogaster*. *Genetics* **125,** 41–50 (1990).
18. Lee, E. C. & Baker, N. E. gp300sca is not a high affinity Notch ligand. *Biochem. Biophys. Res. Commun.* **225,** 720–725 (1996).
19. Kidd, S., Baylies, M. K., Gasic, G. P. & Young, M. W. Structure and distribution of the Notch protein in developing *Drosophila*. *Genes Dev.* **3,** 1113–1129 (1989).
20. Fehon, R. G. *et al.* Complex cellular and subcellular regulation of Notch expression during embryonic and imaginal development of *Drosophila*: Implications for Notch function. *J. Cell. Biol.* **113,** 657–669 (1991).
21. Wesley, C. S. Notch and wingless regulate expression of cuticle patterning genes. *Mol. Cell Biol.* **19,** 5743–5758 (1999).
22. Hart, A. C., Krämer, H. & Zipursky, S. L. Extracellular domain of the boss transmembrane ligand acts as an antagonist of the sev receptor. *Nature* **361,** 732–736 (1993).
23. Parks, A. L., Klueg, K. M., Stout, J. R. & Muskavitch, M. A. Ligand endocytosis drives receptor dissociation and activation in the Notch pathway. *Development* **127,** 1373–1385 (2000).
24. Lieber, T., Kidd, S., Alcamo, E., Corbin, V. & Young, M. W. Antineurogenic phenotypes induced by truncated Notch proteins indicate a role in signal transduction and may point to a novel function for Notch in nuclei. *Genes Dev.* **7,** 1949–1965 (1993).
25. Rebay, I. *et al.* Specific EGF repeats of Notch mediate interactions with Delta and Serrate: implications for Notch as a multifunctional receptor. *Cell* **67,** 687–699 (1991).
26. Ju, B.-G. *et al.* Fringe forms a complex with Notch. *Nature* **405,** 191–195 (2000).

27. Jennings, B., Preiss, A., Delidakis, C. & Bray, S. The Notch signalling pathway is required for *Enhancer of split* bHLH protein expression during neurogenesis in the *Drosophila* embryo. *Development* **120,** 3537–3548 (1994).
28. Wesley, C. S. & Saez, L. Analysis of Notch lacking the carboxyl terminus identified in *Drosophila* embryos. *J. Cell. Biol.* **149,** 683–696 (2000).
29. Blaumueller, C. M. *et al.* Intracellular cleavage of Notch leads to a heterodimeric receptor on the plasma membrane. *Cell* **90,** 281–291 (1997).

Acknowledgements

We thank S. Artavanis-Tsakonas, N. Baker, K. Fischbach, T. Lieber, M. Mlodzik, M. Muskavitch and M. Young for strains and reagents; L. Saez for help with S2 cell transfections; S. Kidd for cell-surface biotinylation protocol; R. Kopan, E. Newberry, D. Towler, D. Ornitz, M. Tondravi, Y. Kasai, J. Skeath and members of the Cagan laboratory for discussions and comments on the manuscript. This work was supported by the NIH, NSF, a Research Associate Fellowship from the McDonnell Center for Cellular and Molecular Neurobiology (P.A.P.), and an NIH grant to M. Young (C.S.W.).

Correspondence and requests for materials should be addressed to R.L.C. (e-mail: cagan@molecool.wustl.edu).

Polarity controls forces governing asymmetric spindle positioning in the *Caenorhabditis elegans* embryo

Stephan W. Grill*†, Pierre Gönczy*‡, Ernst H. K. Stelzer* & Anthony A. Hyman†

** European Molecular Biology Laboratory (EMBL), D-69117 Heidelberg, Germany*
† Max-Planck-Institute for Cell Biology and Genetics (MPI-CBG), D-01307 Dresden, Germany

Cell divisions that create daughter cells of different sizes are crucial for the generation of cell diversity during animal development[1]. In such asymmetric divisions, the mitotic spindle must be asymmetrically positioned at the end of anaphase[2,3]. The mechanisms by which cell polarity translates to asymmetric spindle positioning remain unclear. Here we examine the nature of the forces governing asymmetric spindle positioning in the single-cell-stage *Caenorhabditis elegans* embryo. To reveal the forces that act on each spindle pole, we removed the central spindle in living embryos either physically with an ultraviolet laser microbeam, or genetically by RNA-mediated interference of a kinesin[4]. We show that pulling forces external to the spindle act on the two spindle poles. A stronger net force acts on the posterior pole, thereby explaining the overall posterior displacement seen in wild-type embryos. We also show that the net force acting on each spindle pole is under control of the *par* genes that are required for cell polarity along the anterior–posterior embryonic axis. Finally, we discuss simple mathematical models that describe the main features of spindle pole behaviour. Our work suggests a mechanism for generating asymmetry in spindle positioning by varying the net pulling force that acts on each spindle pole, thus allowing for the generation of daughter cells with different sizes.

The first cleavage division of *C. elegans* embryos generates a large anterior and a smaller posterior blastomere along the anterior–posterior axis[5]. Polarity in this system is established after fertilization[6] by the concerted action of at least six *par* genes[7]. During anaphase B, the spindle elongates asymmetrically: the anterior spindle pole remains in a relatively fixed position along the anterior–posterior axis, while the posterior spindle pole is displaced towards the posterior of the embryo as it oscillates transversely[8].

Two types of microtubule-dependent forces contribute to spindle positioning and elongation during anaphase B in other systems[9–12]. First, overlapping spindle microtubules can generate forces that 'push' spindle poles apart[9]. Second, forces transmitted by astral microtubules can 'pull' spindle poles apart[10–12]. To test which of these apply to the one-cell *C. elegans* embryo, we removed the spindle midzone that connects the two spindle poles at the beginning of anaphase B, and examined the resulting movement of the two independent spindle poles. If intra-spindle forces alone drive anaphase B, then the two spindle poles should not separate after the spindle is severed. In contrast, if extra-spindle pulling forces participate in anaphase B, separation of the two spindle poles should still occur after severing. The spindle midzone was severed with a pulsed ultraviolet laser microbeam, or removed by RNA mediated interference (RNAi)[4] of a *C. elegans* kinesin that is related to XKCM1/MCAK[13–16] (referred to as CeMCAK). In both experimental situations, we verified the disappearance of the spindle midzone by immunofluorescence with anti-tubulin antibodies (Fig. 1b, c; compare with Fig. 1a, arrows). The effect was spatially confined, as astral microtubules were not affected (Fig. 1b, c; compare with Fig. 1a, arrowheads).

We tracked each spindle pole using time-lapse differential interference contrast (DIC) microscopy. This showed both a dramatic increase in pole to pole distance (Fig. 2b, c; compare with Fig. 2a, arrowheads) and an increase in peak velocities of the spindle poles (Fig. 3) after removal of the spindle. Together, these results demonstrate that forces external to the spindle act on the spindle poles during anaphase B. Notably, in both of the experimental situations, the posterior spindle pole behaved differently compared with the anterior one (Figs 2 and 3). The posterior pole covered a greater distance, travelled at about a 40% higher peak velocity, and underwent transverse oscillations in the proximity of the cell cortex. This suggests that a greater pull acts on the posterior spindle pole than on its anterior counterpart, which may explain the overall posterior displacement of the spindle during anaphase B in wild-type embryos. Formally, a change in viscous drag could account for the observed differences in peak velocities, although this is unlikely, on the basis of an analysis of yolk-granule motion (see Methods).

We next examined how the *par* genes influence the net pulling

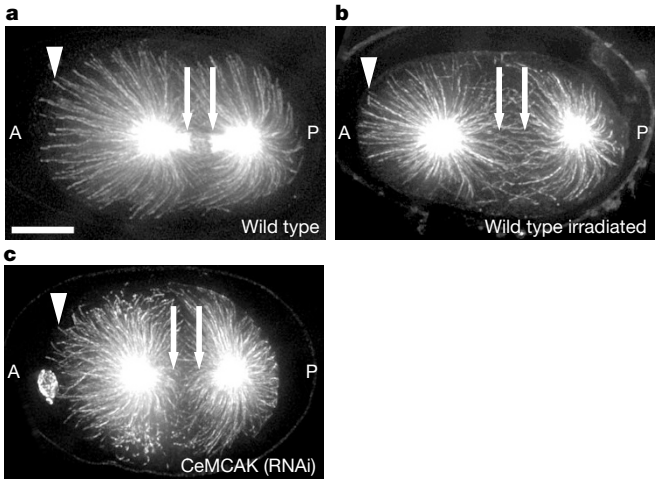

Figure 1 Spindle midzone viewed by indirect immunofluorescence with anti-tubulin antibodies. All embryos are in anaphase B. Anterior (A) is on the left and posterior (P) is on the right in this and all other figures. Scale bar, 10 μm. **a**, In wild-type embryos, both the spindle microtubules (arrows) and astral microtubules (arrowheads) are visible. **b**, **c**, Both in the wild-type irradiated and in the CeMCAK (RNAi) embryos astral microtubules are visible (arrowheads), but spindle microtubules are not (arrows).

‡ Present address: Swiss Institute for Experimental Cancer Research (ISREC), CH-1066 Lausanne, Switzerland.